Proceedings of ASME Turbo Expo 2019: Turbomachinery Technical Conference and Exposition
GT2019
June 17-21, 2019, Phoenix, Arizona, USA

DRAFT **GT2019-91788**

EVALUATING THE USEFULNESS OF RANS IN FILM COOLING

Fraser B. Jones, Dale W. Fox, and David G. Bogard
The University of Texas at Austin
Austin, Texas, USA

Thomas E. Dyson
GE Global Research
Niskayuna, New York, USA

Zachary Webster
GE Aviation
Cincinnati, Ohio, USA

Abstract

Film cooling is a very common technique used in cooling turbine engine components, and hence has been studied extensively experimentally and computationally. Computational studies of film cooling range from more simplistic RANS predictions to high fidelity LES predictions. Generally the accuracy of computational predictions of film cooling is evaluated based on the adiabatic effectiveness measured and predicted downstream of the hole. For this study, a RANS computational prediction was used, but he evaluation of the accuracy of the prediction was based on measured thermal and velocity fields within the coolant hole and immediately downstream. We chose a relatively complex film cooling configuration consisting of a row of 7-7-7 shaped holes fed by an internal channel flow with a range of internal crossflow velocities and coolant jet velocities. Previous experimental studies using this configuration showed that at various inlet velocity ratios, the coolant jet becomes biased to one side of the diffusing section of the hole, which degrades performance and can cause ingestion into the hole. For this study we wanted to determine the capability of a RANS computation to correctly predict the flow structures, coolant jet biasing, and film effectiveness for this configuration. Computational results were compared to thermal field measurements made with a micro-thermocouple probe, velocity field measurements made with a PIV, and film effectiveness measurements made with an IR camera. These measurements were made within the coolant hole, at the downstream edge of the hole, and at 5*D* downstream of the hole. Results from this study show that the RANS computations accurately predicted the flow and thermal fields within and at the downstream edge of the hole, but failed to predict the evolutions of the thermal field and film effectiveness downstream of the hole.

INTRODUCTION

Modern gas turbines develop high thermal efficiencies by increasing the combustor exit temperatures far in excess of the downstream component's material limitations [1]. Effective internal and film cooling of downstream components is critical to preventing component failure while meeting manufacturer goals for reliability and efficiency. Engine efficiency is principally driven by increasing turbine inlet temperatures and decreasing the compressor bleed for thermal protection of the hot end components [1]. More efficient use of coolant permits achieving both goals but requires more advanced internal geometry and film cooling optimization. Generally, the development of new film cooling hole geometries relies on experimental testing since computational predictions with simple RANS codes often provide inaccurate results [2]. DNS and LES computational analyses have proven effective at predicting performance of some film cooling configurations [1,3-5], but remains expensive and time consuming.

The goal of this study was to more thoroughly investigate the capabilities and limitations of RANS codes, with appropriate turbulence models, to predict film cooling performance. A unique aspect of this study was the investigation of the coolant flow within a shaped cooling hole. Evaluations were done by comparing to experimental measurements of velocity and thermal fields within and a short distance downstream of the coolant hole, and film cooling effectiveness measurements downstream of the hole. Results from an iLES simulation were also used to evaluate predictions of separation regions within the coolant hole. A 7-7-7 forward expanded, fan-shaped hole was used in this study. Two coolant feed configurations were used, a plenum and an internal channel flow. The configuration including the internal flow channel provided a test case which involved a complex flow pattern at the inlet of the hole, so served as a particularly challenging test case.

NOMENCLATURE

Cd	Discharge coefficient
d	Film cooling hole diameter
DR	Density ratio, ρ_c/ρ_∞
l	Channel length
M	Blowing Ratio
P	Pitch

p Pressure
R Ideal gas constant for air
Re_d Reynolds number, $\rho_\infty u_\infty d/\mu_\infty$
T Temperature
U Velocity magnitude
VR Velocity ratio
VR injection velocity ratio $Uj/U\infty$
VR_c crossflow velocity ratio $Uc/U\infty$
VR_i inlet velocity ratio Uc/Uj
W Channel width
x Stream-wise coordinate
y Wall normal coordinate
z Span-wise coordinate

GREEK
α Hole inclination angle
β Lateral expansion angle
γ Ratio of specific heats, forward expansion angle
δ Boundary layer thickness, uncertainty
η Adiabatic effectiveness
ρ density
φ Overall effectiveness

SUBSCRIPTS
Avg Averaged
Aw Adiabatic wall
c Channel
cl Centerline
f Film cooling
i Hole inlet
j Coolant jet in metering section
in Channel inlet
t Total

Description of Experimental and Numerical Processes

Experimental measurements used in this study were done using a flat plate test configuration with film cooling holes fed by an internal cross-flow channel. This facility has been used in several previous studies including [6,7]. The measurements used for evaluating numerical results were velocity fields, thermal fields, and surface adiabatic effectiveness measurements. All experimental results presented in this paper were presented previously in either [6] or [7]. Numerical predictions were done using the commercial Fluent code, version 17.2. Details of numerical simulations are described below.

Summary of experimental facilities and procedures. Detailed descriptions of the experimental facilities and procedures are presented in [6,7], and only a brief summary is presented here. A schematic of the flat plate test section in the recirculating wind tunnel facility used for these experiments is shown in Figure 1. An upstream parallel bar freestream turbulence generator was set to provide a freestream turbulence of Tu_∞ = 4.8% at the coolant hole position. The upstream suction

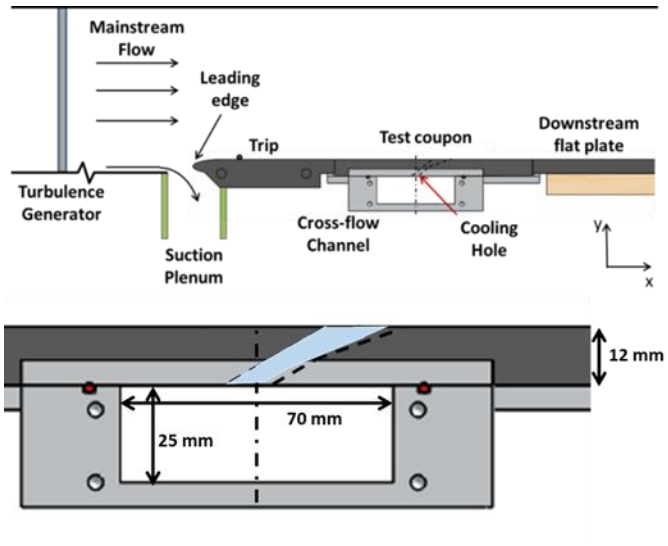

Figure 1. Schematic of test section and internal cross-flow channel.

plenum removed the upstream boundary layer so that a new approach boundary layer was set at the flat plate leading edge. A 3 mm trip was placed upstream of the holes to obtain a turbulent boundary layer thickness of 2.9d at the hole. Also shown in Figure 1 is the cross-section of the internal cross-flow channel. This channel had 6d x 18d cross-section which is representative of internal cooling channels in a turbine blade. Coolant flow in the internal channel was variable from 0.2 to 0.6 of the mainstream velocity. The coolant hole was the baseline 7-7-7 shaped hole [8], shown schematically in Figure 2, with a metering hole diameter of 4.0 mm. The test coupon had a row of eight holes spaced with a pitch between holes of p/d = 6.

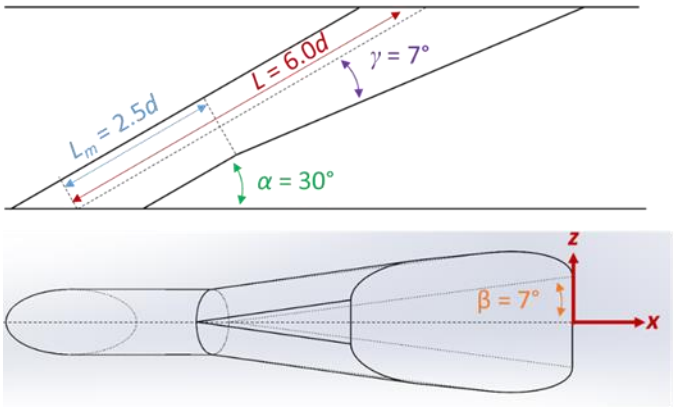

Figure 2. Schematic of the 7-7-7 shaped hole.

A TSI 2D PIV system was used for velocity measurements. This system consisted of a Litron Lasers L135-15 PIV dual ND:YAG laser which was pulsed in coordination with a TSI Powerview Plus CCD camera with a pixel resolution of 1600x1200. A telephoto lens with a focal length of 180 mm and a maximum aperture of f/3.5 was used to view the measurement planes. Measurements were made in three cross-sectional planes

as shown in Figure 3. The plane in the hole was angled at nominally 30° from the vertical so that it was normal to the axial flow direction within the coolant hole, and aligned with the upstream edge of the coolant hole at the external surface. The other two planes were vertical at positions of x/d = 0 and 5 downstream of the coolant hole downstream edge.

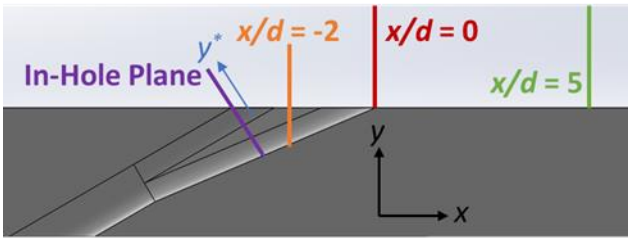

Figure 3. Location of measurement planes for thermal and velocity field measurements

Thermal field measurements were made using a micro-thermocouple probe with a sensor diameter of 50 μm. Measurements within the coolant hole were made in a vertical plane positioned at x/d = -2 as shown in Figure 3. Measurements were also made in vertical planes located at x/d = 0 and 5 downstream of the coolant hole downstream edge.

Numerical Methods. In order to maximize the use of computational resources, the mainstream and crossflow profiles were pre-calculated in separate simulations and loaded as boundary conditions into the crossflow domain shown in Figure 4. Mainstream initial conditions were computed by simulating 450 mm of upstream flow in a separate simulation. Turbulence of 20% was allowed to decay to the target ~5%, isotropic turbulence while generating the correct boundary layer thickness [9,10]. The crossflow channel was similar but with 500 mm of simulation length and an initial turbulence of 5%. Preparing the simulations in this manner allows for a more realistic approximation of boundary conditions while permitting higher cell density in regions of physical interest.

The solution of this CFD simulation was calculated using a Coupled Pressure-Velocity scheme which greatly enhances the simulation stability at the cost of more than doubling the memory requirements. Spatial discretization was accomplished with a Green-Gauss Node Based gradient scheme to minimize numerical diffusion and spurious residuals. Pressure was solved to second order while Momentum, Turbulent Kinetic Energy, Turbulent Dissipation Rate, and Energy were solved using a third order MUSCL scheme. MUSCL provides third order accuracy for unstructured domains meshes but little improvement over second order schemes for structured domains. Early meshes were all unstructured, but advances in ANSYS CutCell meshing technique allowed for the generation of accurate, structured meshes. MUSCL schemes were retained for consistency to older work after concluding it had no negative impact on a structured mesh. Turbulence modeling were done using the Realizable k-ε model with enhanced wall modeling, curvature correction, and pressure correction.

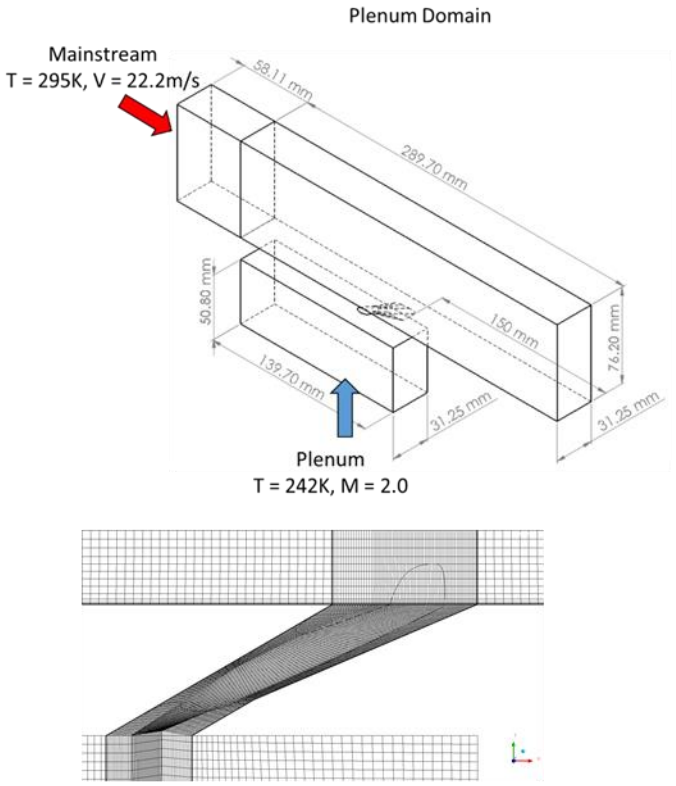

Figure 4. Domain and meshing used to simulate the plenum fed coolant holes.

Domain and Grid. Linear periodicity was used to limit the domain size to one full hole at the center of one pitch. The mainstream was bound in the vertical direction by a zero-shear plane located at a height equal to half the height of the wind tunnel. A minimum of 20 diameters upstream and downstream of the hole were used to minimize any effects of the boundary conditions on the physics of the coolant-mainstream interaction.

Two gridding methods were used. The computational domain for the plenum fed holes, the Plenum domain, was meshed in ICEM using structured mesh with an O-Grid for the hole. Prism layers were used to increase mesh density near the hole and mainstream wall. Total cell count was 2.3 million, with maximum cell size of 2 mm.

ANSYS meshing cut-cell and free tetrahedral meshing were used for the cross-flow case. Presented here is the structured cut-cell mesh. Three distinct regions of mesh resolution were defined to maximize the use of computational resources. In-hole, entrance, and outlet effects were captured with a 100 μm cell size. Slightly upstream of the hole outlet and the entire downstream region were captured at 400 μm resolution, while the remaining area was filled with an 800 μm mesh. The mainstream, channel, and hole walls were all refined with a prism layer bringing the wall normal mesh height to 1μm. The variation in prism layer height comes from specifying the prism growth to stop at an aspect ratio of 1 which, for cut-cell meshing, is equal to the local mesh size. The total cell count for the crossflow simulation was 5 million. Tests of 7, 10, and 11 million

cell meshes were conducted to identify the minimum resolution necessary for grid independence.

Boundary conditions. A series of simulations were used to establish the mainstream turbulence characteristics matching the experimental facility. A mentioned previously, increased mainstream turbulence in the wind tunnel facility was generated using a parallel bar grids. Measurements showed that the turbulence level decay downstream of this grid matched the correlation from Roach [11]. For the numerical simulation of the decaying mainstream turbulence, a 450 mm long CFD domain of equal dimension to the wind tunnel height and 1 pitch wide with symmetry in the lateral direction was used. The inlet to this computational domain corresponded to a position 70 mm downstream of the bar grid. At this position the Roach correlation predicted a turbulence level of 20%, which was used as the inlet condition for the simulation of the mainstream turbulence decay. The decay rate of turbulence is sensitive to the turbulence length scale, and for this simulation the inlet turbulence length scale was varied until turbulence decay matched the prediction of the Roach correlation as shown in Figure 6. This matching occurred when the inlet turbulence length scale was 8.5 mm, which corresponded well with the measured turbulence integral length scale of 10 mm.

The predicted turbulent boundary layer growth along the 450 mm length upstream of the coolant holes was found to match the measured approach boundary layer thickness of 2.9d. For the numerical simulation of the internal cross-flow channel, an approach length of 500mm length before the crossflow domain inlet was used. The velocity profile across the channel was found to match well with the experimental measurements, with an internal turbulence level of 5%.

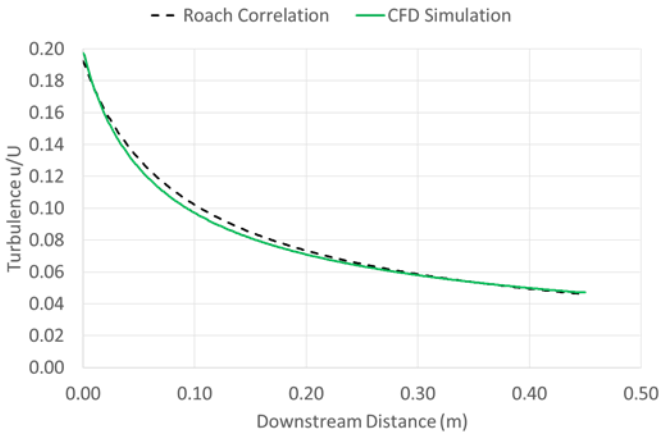

Figure 6. Comparison of mainstream turbulence decay predicted using Fluent code with the Roach correlation [11].

RESULTS

Evaluations of RANS computational predictions were done for a plenum fed 7-7-7 shaped hole and a 7-7-7 shaped hole fed from an internal cross-flow channel with varying channel velocities. Results from these evaluations are presented below.

Evaluation of RANS predictions of internal flows within shaped holes. The primary focus of the evaluation of the RANS prediction of a plenum fed 7-7-7 shaped hole was the flow within the coolant hole, particularly the separation regions within the hole. Not surprisingly there is no experimental data for this internal flow field, but there was a recent high fidelity computational study using iLES [3] which provides a detailed average velocity field within a plenum fed 7-7-7 shaped hole. The operating conditions for this simulation were hole Reynolds number of Re_d = 6,000, coolant density ratio DR = 1.6, blowing ratio of M = 2.0, and mainstream Mach number of Ma = 0.06. The RANS simulation of this same geometry was done for similar operating conditions, except the density ratio was DR = 1.2.

Predictions of the in-hole velocity fields from the iLES study in the literature [3] and the RANS simulation are presented in Figure 7. Immediately apparent in comparing the two computational predictions is the streamline patterns and separation regions are very similar for the two simulations. One would expect that the RANS computation to predict the separation region at the inlet of the hole because of the sharp corner at the downstream edge of the hole inlet. Not only did the RANS predict this separation, but the predicted size of the separated region was very similar to the iLES simulation. Furthermore, the RANS computation predicted a separation region on the diffuser section which was very similar in size to that predicted by the iLES. Finally the streamline pattern above the separation regions and exiting the hole were very similar for both simulations. Of course the performance of the shaped hole is significantly affected by these separation regions, so the successful prediction by the RANS simulation is indicative that these more simplistic computational prediction will give useful insight in the performance of shaped film cooling holes.

Evaluation of RANS predictions of film cooling with shaped holes fed by internal cross-flow channels. RANS predictions for a 7-7-7 shaped film cooling hole fed by an internal channel with cross-flow were evaluated by comparison to experimental measurements. These measurements included discharge coefficients for the holes, thermal fields and velocity fields within the hole, at the hole exit, and downstream of the hole, and adiabatic effectiveness downstream of the hole.

The discharge coefficient, C_d, was predicted with the RANS simulation, and compared to experimental measurements in our laboratory [6]. These C_d values were determined from measurements of static pressure at the inlet of the hole, P_c, and at the exit of the hole, P_∞, the coolant temperature, T_c, and the mass flow rate through the coolant hole, $\dot{m}$, using the following equation:

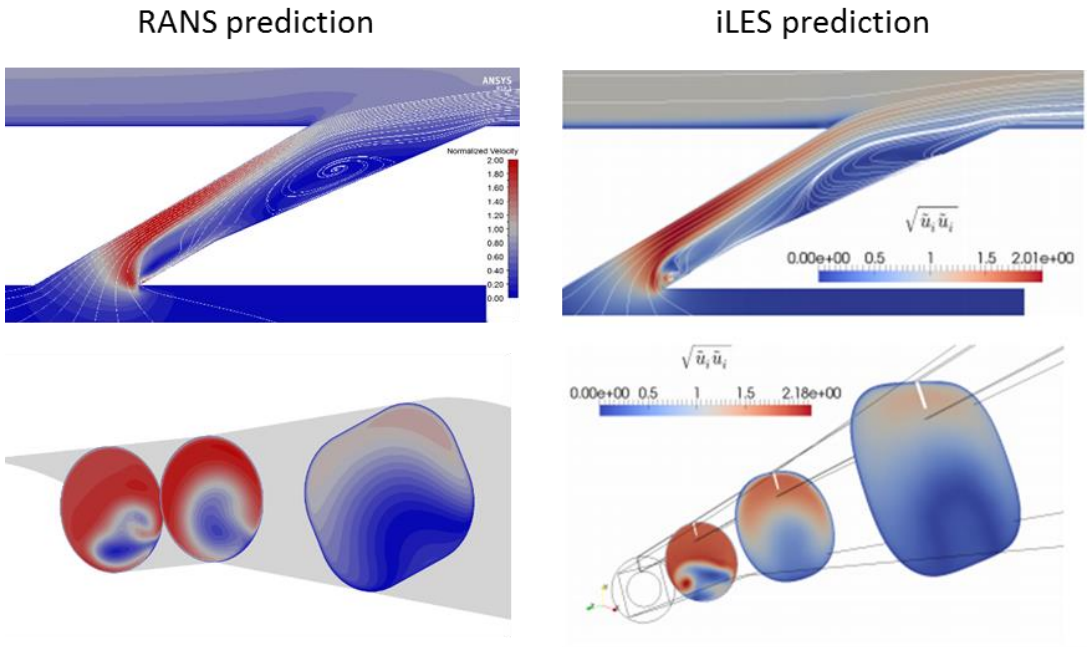

Figure 7. Comparison of RANS and iLES predictions of the mean velocity distributions within the 7-7-7 shaped coolant hole along the centerline of the hole.

Comparison of the predicted and measured C_d values for varying coolant velocity ratios is given in Figure 8 for the case with VR_c = 0.4. The predicted C_d distribution followed trend similar to the experimental measurements, but were nominally about 10% lower.

$$C_d = \frac{\dot{m}}{\frac{\pi}{4} D^2 P_c \left(\frac{P_\infty}{P_c}\right)^{\frac{\gamma+1}{2\gamma}} \sqrt{\frac{2\gamma}{(\gamma-1)RT_c}\left(\left(\frac{P_c}{P_\infty}\right)^{\frac{\gamma-1}{\gamma}} - 1\right)}} \qquad [12]$$

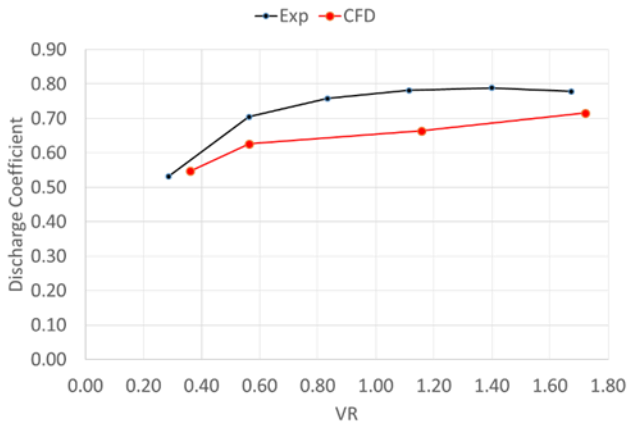

Figure 8. Comparison of predicted and measured C_d distributions with varying VR, and VR_c = 0.4.

Experimental measurements of the thermal fields associated with film cooling using 7-7-7 shaped holes fed by an internal cross-flow channel were made within the coolant holes and at x/d = 0 and 5 downstream of the holes (previously published in [5]). These measurements showed that the channel cross-flow at the inlet of the holes caused a significant skewing of the coolant flow through the hole and the coolant jet exiting the hole. The jet skewing was found to be a function of the channel/jet velocity ratio defined as $VR_i = V_c/V_j = VR_c/VR$, with maximum jet skewness occurring at VR_i = 0.36. These data were used as a particularly stringent test in evaluating the RANS computations.

Comparisons between experimental measurements and RANS computational predictions of the thermal fields within and above the coolant holes at x/d = -2 are shown in Figure 9 for four combinations for VR and VR_c. In each case the thermal fields show regions where the coolant temperature is still at the inlet temperature, i.e. $\theta = 1.0$, and interface at the hole exit where gas temperature rise to the mainstream temperature, i.e. $\theta = 0$. This figure shows that there was a remarkable correspondence between the RANS computational predictions and the measurements for all cases. For the lower velocity ratio cases, VR = 0.56/VR_c = 0.4 and VR = 0.83/VR_c = 0.6, the measured thermal profiles clearly show a dip in the thermal interface at the middle of the hole. As noted by McClintic et al. [7], the dip the thermal interface in the middle of the hole is believed to be due rotation in the flow at the hole inlet due to the cross-flow in the channel feeding the hole. For the lower VR the relative strength of the cross-flow is greater resulting in a stronger rotation that brings coolant back to the right side of the hole. For these cases, the RANS computation showed a dip the thermal interface at the

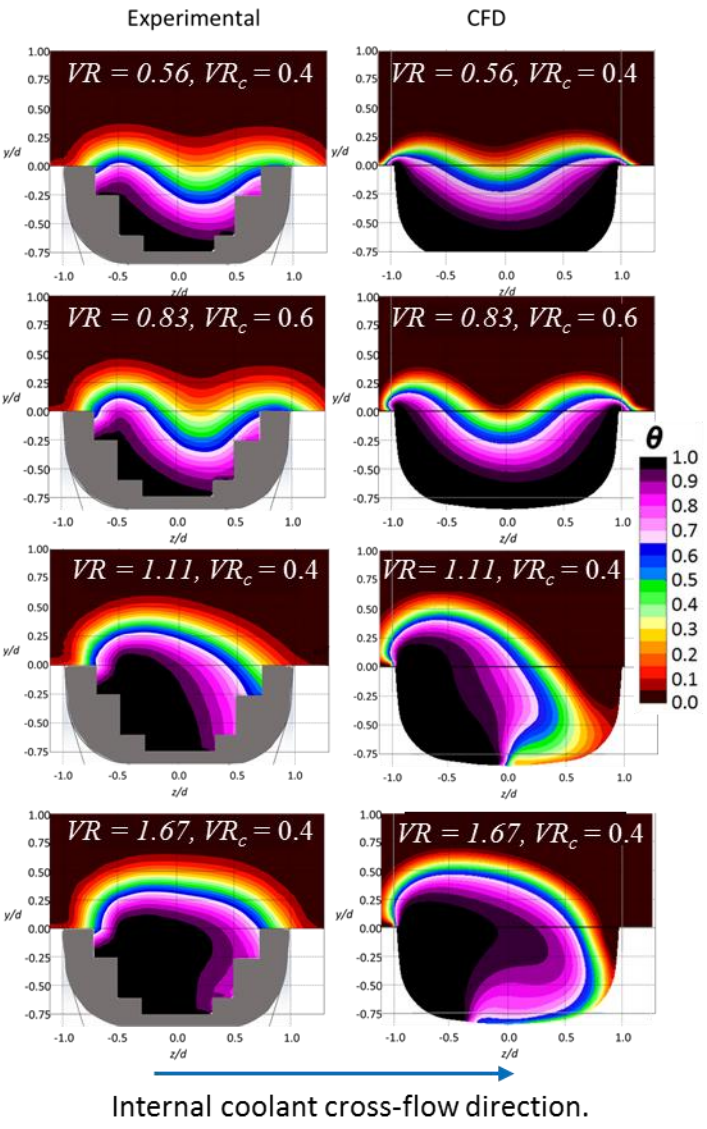

Figure 8. Comparisons of experimental and CFD predictions of the thermal fields within and above the coolant hole at *x/d* = -2.

middle of the hole very similar to the experimental measurements.

For the higher velocity ratio cases, $VR = 1.11/VR_c = 0.4$ and $VR = 1.67/VR_c = 0.4$, measurements showed the internal coolant skewed to the left side of the hole. Note that the internal cross-flow direction is from left to right, so the coolant flow would impact on the right side of the hole inlet, and then swirls to the left side as it exits the hole. This results in ingestion from the mainstream into the hole on the right side. Again the thermal fields from the RANS computational prediction are very similar to the experimental measurements. This shows that the RANS computations were able to predict key characteristics of flow through the shaped coolant hole including complex flow patterns generated by strong cross-flow at the inlet to the hole.

As noted earlier, a PIV system was used to measure the velocity field in the cross-section within the coolant hole aligned normal to the hole axis. Computational predictions were made in this same plane, and these results are compared to experimental measurements in Figure 10 (a) for $VR = 0.56/VR_c$

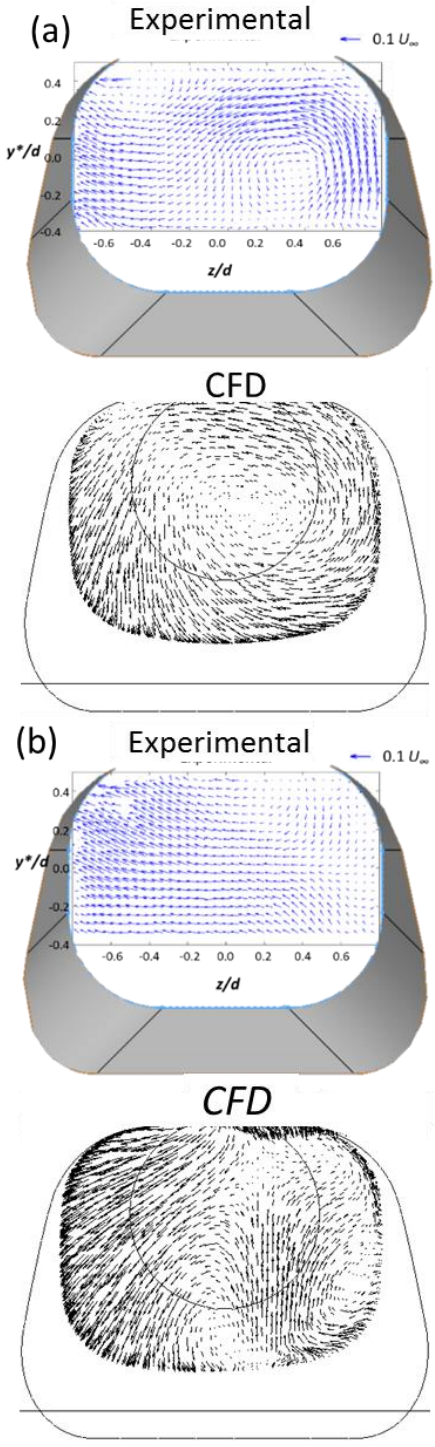

Figure 10. Comparisons of experimental and CFD predictions of in-hole velocity fields for VR_c = 0.4 and (a) VR = 0.56, and (b) VR = 1.11.

= 0.4 and Figure 10 (b) for $VR = 1.11/VR_c = 0.4$. These two cases correspond to flow conditions which result in a broad thermal field and a highly skewed thermal field at the exit of the hole, respectively. For the $VR = 0.56/VR_c = 0.4$ case, the measurements showed a rotational flow on the right side of the hole with an uplifting motions along the wall of the hole on the right side. The RANS simulation showed a similar rotational flow that was skewed to the right side of the hole. There was disagreement between experiment and CFD on the left side of the hole where measurements a flow towards the left side of the hole, while RANS simulations showed a strong downward motion. For the $VR = 1.11/VR_c = 0.4$ case, measurements and CFD prediction were similar in showing an upward flow on the right side of the hole. However, on the left side of the hole, measurements showed flow to the left with a slight upward trajectory, while RANS simulations predicted a flow towards the left with a strong downward movement. These results show that the RANS simulation predicted general flow trends similar to the measurements, but there were clear differences.

Cross-sections of the velocity field were also measured at $x/d = 0$ and 5, and these measurements are compared with CFD RANS predictions in Figures 11 (a) and (b) for flow conditions of $VR = 0.56/VR_c = 0.4$, and $VR = 1.11/VR_c = 0.4$, respectively. For the lower velocity ratio case, Figure 11 (a), the velocity

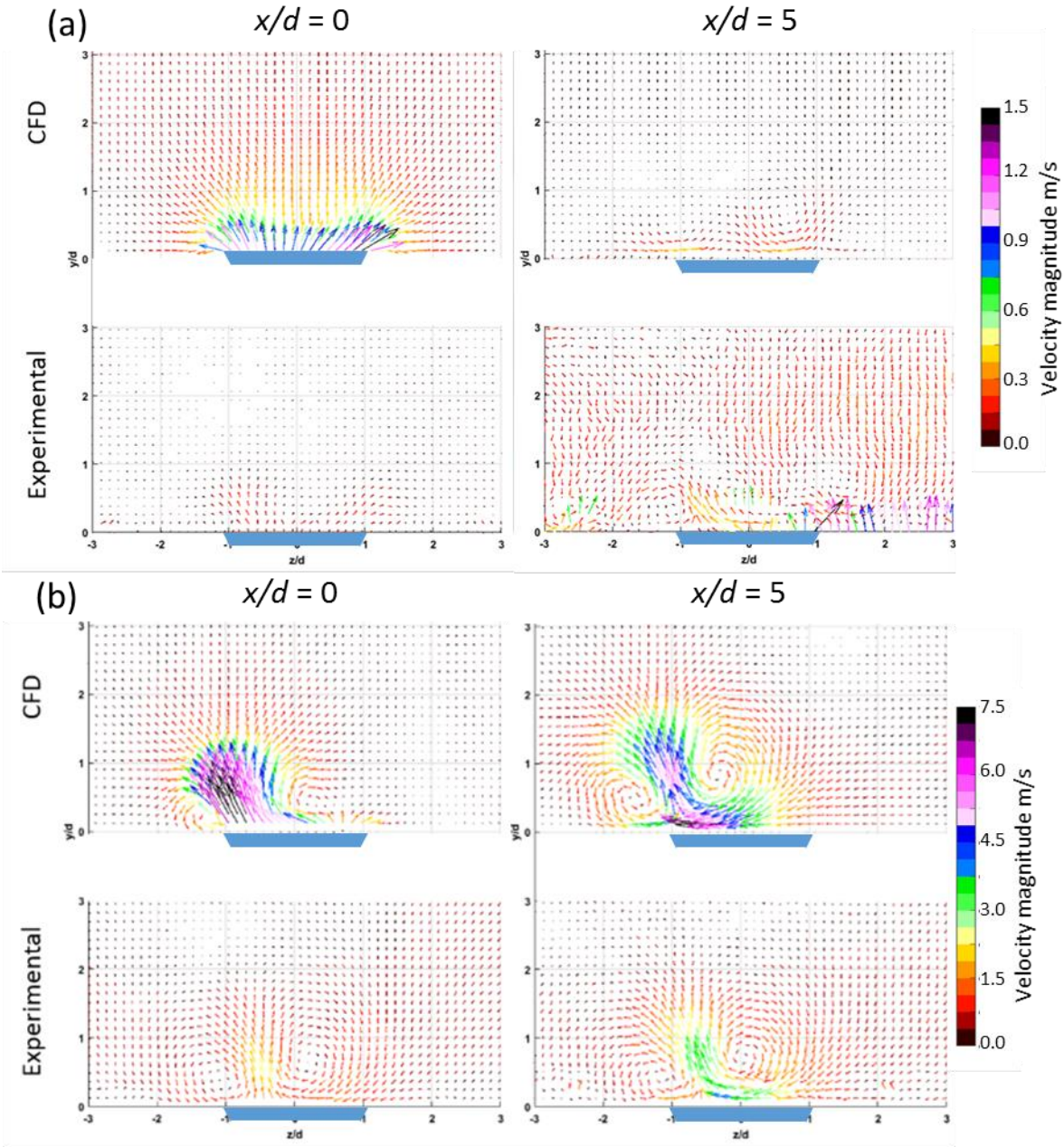

Figure 11. Comparisons of experimental and CFD predictions of velocity fields downstream of the hole for $VR_c = 0.4$ and (a) $VR = 0.56$, and (b) $VR = 1.11$.

measurements showed little effects on the velocity vectors in the cross-flow planes at either x/d = 0 and 5. The CFD predictions also showed negligible effects at x/d = 5, but at x/d = 0 the CFD prediction showed a vertical velocity component at the exit of the hole, albeit only 1 m/s, i.e. 0.04 U_∞. For the higher velocity ratio case, VR = 1.11/VR_c = 0.4, Figure 11 (b), the velocity vectors shows similar flow fields for the experiment and CFD prediction in which a slanted jet exits from the left side of the hole at an slightly off of vertical, with counter rotating vortices on either side of this jet. However, the CFD prediction had velocity vectors which were two to three times larger in magnitude than the measured velocities.

Cross-sections of the thermal fields measured and predicted with the RANS simulations at x/d = 0 and 5, are compared in Figures 12 (a) and (b) for flow conditions of VR = 0.56/VR_c = 0.4, and VR = 1.11/VR_c = 0.4, respectively. These thermal fields are superimposed over the velocity vectors discussed previously to show the correlation between the thermal fields and the velocity fields. For the lower velocity ratio case, Figure 12 (a), coolant flow at the downstream edge of the coolant hole, x/d = 0, was relatively uniform with a double peak pattern with peaks at each end of the hole. The RANS CFD prediction had a very

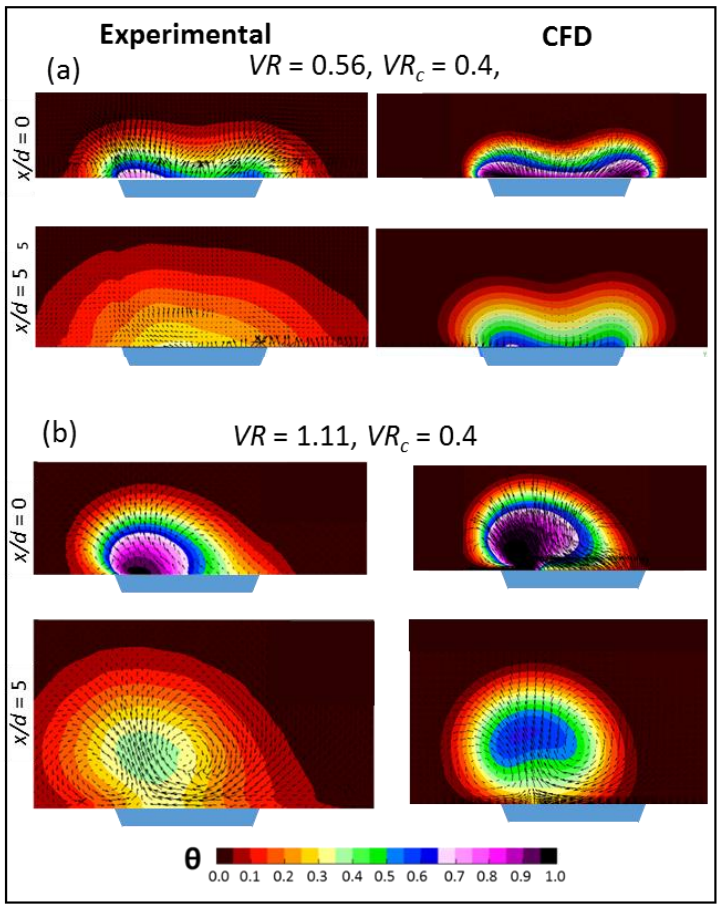

Figure 12. Comparisons of experimental and CFD predictions of thermal fields downstream of the hole for VR_c = 0.4 and (a) VR = 0.56, and (b) VR = 1.11.

similar pattern at this position, although significantly higher peak θ values near the wall. Farther downstream at x/d = 5, there were significant differences between experimental measurements and CFD predictions. The measurements showed a broad distribution of coolant, and no hint of a double peak pattern. The CFD prediction had much less lateral and vertical dispersion of the coolant, much higher θ values in the core of the coolant jet, and still had a distinct double peak pattern.

For the higher velocity ratio case, Figure 12 (b), there was a distinct bias in the coolant distribution exiting the hole at x/d = 0, with a strong core of coolant on the left side of the hole. This is consistent with the in-hole thermal field measurements, and the velocity field measurements discussed previously. The CFD prediction at this location is very similar to the measured distribution, though with a larger θ = 1 jet core which was slightly farther from the surface. However, at x/d = 5 there was again a significant difference between the measured and computationally predicted thermal fields, with the measured thermal field showing significantly more dispersion in the lateral and vertical directions. Both experimental measurements and CFD predictions showed the core of the coolant jet distinctly detached from the surface, but the CFD predicted a jet core with $\theta > 0.6$, while the measured core was $\theta < 0.4$.

There was a consistent trend in the CFD predicted thermal fields downstream of the coolant hole for the two operating conditions with low and high coolant jet velocity ratios. In both cases the predicted thermal fields at the downstream edge of the coolant hole was very similar to the measured distribution. But as the coolant jet travelled downstream over the range from x/d = 0 to x/d = 5, the RANS computations significantly under-predicted the mixing of the coolant jet with the mainstream. Consequently the lateral and vertical dispersion of coolant jet, and the decay of the core temperature of the coolant jet were significantly under-predicted.

The primary measure of film cooling performance is the film effectiveness η defined as follows:

$$\eta = \frac{T_\infty - T_{aw}}{T_\infty - T_c} \qquad (2)$$

where T_∞ is the mainstream temperature, T_{aw} is the adiabatic wall temperature, and T_c is coolant temperature at the hole exit. This is a measure of the coolant temperature immediately above the surface, and hence the effective driving temperature for heat transfer into the wall. Comparisons of measured and CFD predictions of distributions of η downstream of coolant holes for a range of operating conditions is shown in Figure 13. Immediately apparent from this figure is that there were very poor CFD predictions of actual η distributions for all cases. At the lower velocity ratios the CFD predicted much higher η values, but for higher velocity ratios CFD predicted much lower η values. The difference in these two cases was that for lower velocity ratios the coolant jets were well attached, but for higher velocity ratios the cores of coolant jets were detached from the surface. In each case the poor predictions of the dispersion of

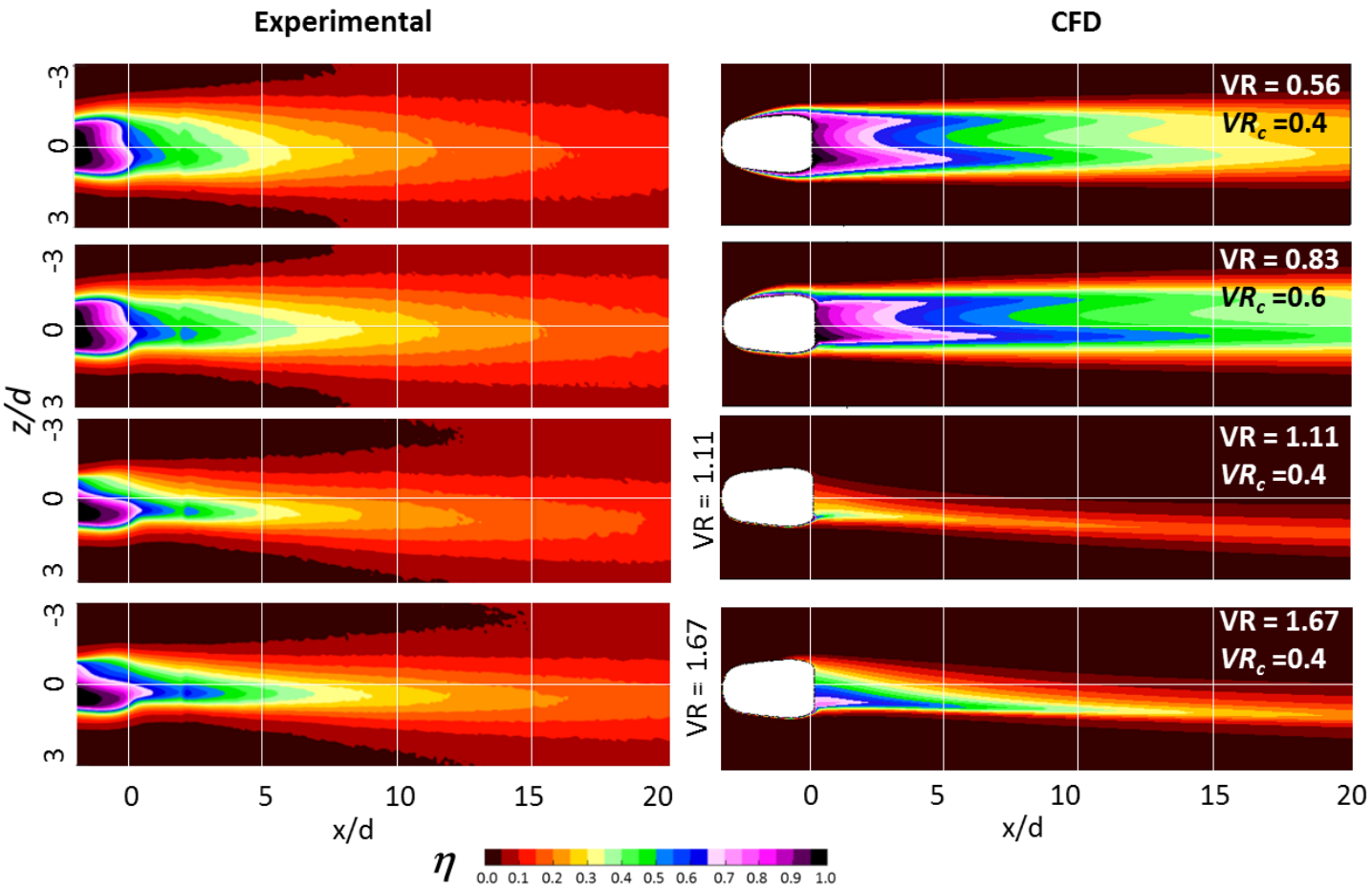

Figure 13. Comparison of experimental and CFD predictions of adiabatic effectiveness for varying *VR* and VR_c.

the coolant caused poor predictions of η values. For the lower velocity ratios with attached coolant jets, the decreased coolant dispersion results in much higher η values in the center of the cooled region which offsets the decreased lateral spreading. For the high velocity ratios with detached coolant jets, the decreased coolant dispersion results in less coolant from the detached core of the coolant jet being transported to the surface, and hence decreased η values. This is particularly evident in the thermal fields shown in Figure 12 (b) which show that although the predicted core of the coolant jet has much higher θ values than the actual jet core, the θ values measured near the wall were much higher, which can be attributed to the turbulent diffusion of the coolant gas that is under-predicted by the CFD simulation.

Considering the reasonably accurate CFD predictions for coolant flow within the shaped hole, the mechanisms that caused a double peak pattern of coolant flow at low *VR*, but an extreme skewing of the jet for high *VR*, were investigated by tracking predicted streamlines flowing from the internal cross-flow channel into and through the coolant hole. Results from this analysis are shown in Figure 14 (a) and (b) for flow conditions of $VR = 0.56/VR_c = 0.4$, and $VR = 1.11/VR_c = 0.4$, respectively. Recall that based on our previous experimental studies [5], we speculated that the vortical rotation at the inlet of the hole caused the coolant jet to swirl to the opposite side of the hole at the higher velocity ratio, and at lower velocity ratio the swirling was enhanced causing the coolant swing back to the other side of the coolant hole. The streamline patterns shown in Figure 14 confirm this hypothesis, showing significantly more swirling for the *VR* = 0.56 cases resulting in streamlines that rotated a full 360° and ultimately exited on the right side of the hole.

CONCLUSIONS

A detailed comparison of RANS with experimental measurements for crossflow shows fidelity levels differ for velocity, pressure, and temperature. Blanket skepticism about the usefulness of RANS may be undeserved. RANS seems to be in strong agreement with velocity fields. Comparision of PIV and thermalfields show RANS can correctly predict biasing of a shaped, crossflow fed cooling hole. Predicting the discharge coefficient follows the experimental trends but overpredicts the pressure loss when biasing is strongest. This may be a general deficiency in RANS or simply a disconnect between the perfect computational geometry and the real, imperfect geometry of an

experimental film cooling hole. Finally, RANS completely fails to predict the mixing and spreading of coolant as it interacts with the mainstream. This may be resolvable with different turbulence modeling but is clearly the weakest part of RANS CFD.

Despite all the limitations, it is clear that the excellent ability of RANS to predict the biasing of a shaped hole fed by crossflow over a range of channel and velocity ratios could be of great use to industry or academics. The low computational cost and high throughput permits the fast screening of new hole designs necessary to make the most of design freedoms offered by additive manufacturing. Future work may improve the models for turbulent mixing and surface interactions which might further improve RANS ability to accurately model film cooling.

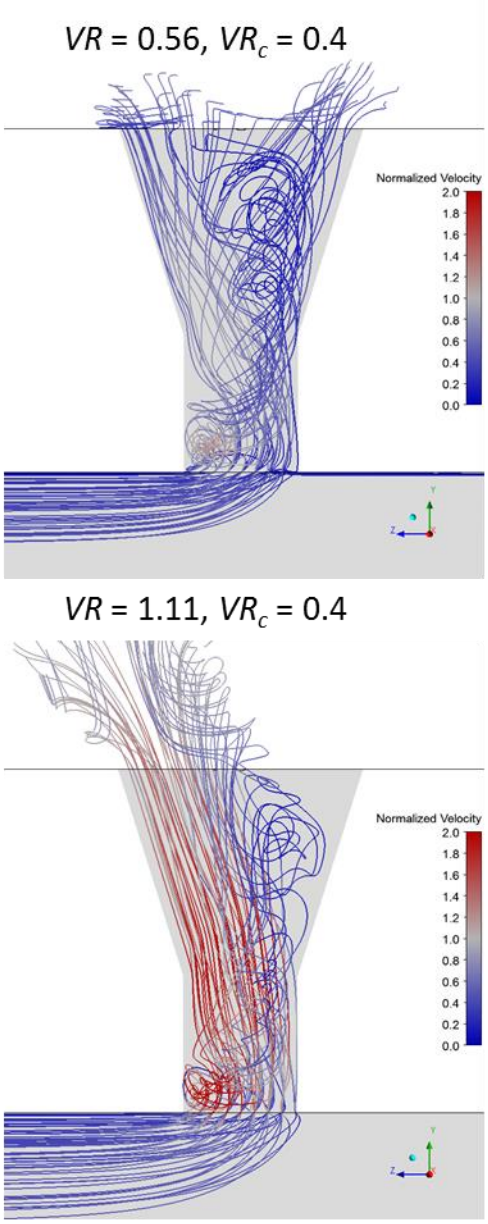

Figure 14. Visualization of inlet streamlines from CFD predictions for VR = 0.56 and 1.11 with channel cross-flow velocity ratio of VR_c = 0.4.

Acknowledgments

The Authors of this paper are grateful for the continued financial and technical support from GE.

References

[1] Bogard, D. G., and Thole, K. A., 2006. "Gas turbine film cooling". *Journal of Propulsion and Power,* **22**(2), pp. 249– 270.

[2] Stewart, W. R., Bogard, D. G., 2014 "Experimental Thermal Field Measurements of Film Cooling Above the Suction Surface of a Turbine Vane". In Proceedings of ASME Turbo Expo 2008: Power for Land, Sea and Air, no. GT2014-27111.

[3] Oliver, T. A., Anderson, J. B., Bogard, D. G., Moser, R. D., and Laskowski, G. 2017. "Implicit LES for Shaped-Hole Film Cooling". In Proceedings of the ASME Turbo Expo 2017: Turbine Technical Conference and Exposition, no. GT2017-63314

[4] Peet, Y. V., and Lele, S. K., 2008. "Near field of film cooling jet issued into a flat plate boundary layer: LES study". In Proceedings of ASME Turbo Expo 2008: Power for Land, Sea and Air, no. GT2008-50420.

[5] Ziefle, J., and Kleiser, L., 2008. "Assessment of a film cooling flow structure by large-eddy simulation". Journal of Turbulence, 9(29), pp. 1–25.

[6] McClintic, J. W., Anderson, J. B., Bogard, D. G., Dyson, T. G., and Webster, Z. D., 2017. "Effect of Internal Crossflow Velocity on Film Cooling Effectiveness – Part I: Axial Shaped Holes". ASME paper No. GT2017-64616.

[7] McClintic, J. W., Fox, D. W., Jones, F. B., Bogard, D. G., Dyson, T. G., and Webster, Z. D., 2017. "Flow Physics of Diffused-Exit Film Cooling Holes Fed by Internal Crossflow". ASME paper No. GT2018-76904.

[8] Schroeder, R. P., Thole, K. A. 2014. "Adiabatic Effectiveness Measurements for a Baseline Shaped Film Cooling Hole" Proceedings of ASME Turbo Expo 2014: Turbine Technical Conference and Exposition GT2014-25992

[9] Anderson, J. B., 2017. "Investigation of Approach Flow Parameters, Scaling Factors, and Measurement Accuracy for Film Cooling Effectiveness and Heat Transfer Coefficient Measurements". PhD Dissertation, University of Texas at Austin, Austin, TX, August.

[10] Anderson, J. B., Boyd, E. J., and Bogard, D. G., 2015. "Experimental investigation of coolant-to-mainstream scaling parameters with cylindrical and shaped film cooling holes". In Proceedings of the ASME Turbo Expo 2015: Turbine Technical Conference and Exposition, no. GT2015-43072.

[11] Roach, P. E., 1986 "The Generation of Nearly Isotropic Turbulence by Means of Grids". *International Journal of Heat and Fluid Flow.* **8**(2), pp. 82-92

[12] Gritsch, M., Schultz, A., and Wittig, S., 2003. "Effect of Internal Coolant Crossflow on the Effectiveness of Shaped Film-Cooling Holes". Journal of Turbomachinery, 125, pp. 547–554.